

Electric charge and strangeness-dependent directed flow splitting of produced quarks in Au+Au collisions

The STAR Collaboration
(Dated: April 7, 2023)

We report directed flow (v_1) of multistrange baryons (Ξ and Ω) and improved v_1 data for K^- , \bar{p} , $\bar{\Lambda}$ and ϕ in Au+Au collisions at $\sqrt{s_{NN}}=27$ and 200 GeV from the STAR at the Relativistic Heavy Ion Collider (RHIC). We focus on particles whose constituent quarks are not transported from beam rapidity rather produced in the collisions. In midcentral collisions, we observe a coalescence sum rule for hadron combinations with identical quark content and a difference (“splitting”) in the slope of v_1 vs. rapidity for combinations having nonidentical quark content. The splitting strength appears to increase with the electric charge difference and strangeness content difference of the constituent quarks in the combinations, consistent with an electromagnetic effect. The peripheral collision statistics are insufficient to draw firm conclusions.

PACS numbers:

Keywords: Directed flow, Electric charge, Strangeness, Heavy-ion collisions, Electromagnetic field

The first harmonic in the Fourier expansion of the azimuthal distribution of emitted particles relative to the reaction plane in a nucleus-nucleus collision [1–3] is known as directed flow, v_1 , a collective sideward motion whose dominant component is an odd function of the particle rapidity (y). The early collision dynamics [4–6] can be probed by $v_1(y)$, an interpretation supported by hydrodynamic [7] and nuclear transport [8] models. The early stage of these collisions features a strong magnetic field, on the order of $10^{14} - 10^{15}$ T [9], dominated by the passing spectator protons. As the charged spectators recede from the collision zone, the magnetic field decreases quickly and the resulting Faraday induction produces an electric current. The charged spectators also exert a Coulomb force on the charged constituents. Meanwhile, the collision zone expands in the longitudinal (beam) direction, which is on average perpendicular to the magnetic field. The Lorentz force moves the particles of the collision zone in opposite directions, depending on their electric charges; this motion is perpendicular to both the longitudinal velocity and the magnetic field, analogous to the Hall effect [10, 11]. The combination of Faraday, Coulomb and Hall effects may influence v_1 of the emitted particles [10–12].

The sign of v_1 splitting can reveal which aspect of the EM field is dominant. When the Hall effect overcomes the Faraday and Coulomb effects, the v_1 of positively charged particles (h^+) at positive rapidity becomes positive, and the opposite happens for h^- . This eventually causes the splitting in v_1 , as illustrated in Fig. 1. The produced medium expands longitudinally, indicated by velocity \vec{u} . The directions of the resultant electric currents due to Faraday, Hall and Coulomb effects are shown. The v_1 directions for h^+ and h^- are illustrated for the case where the Hall current exceeds the Faraday+Coulomb current. When the Faraday+Coulomb effect is stronger, then the v_1 directions for h^+ and h^- are reversed. The v_1 splitting between opposite-charge light hadron pairs like π^\pm , K^\pm , $p - \bar{p}$, etc. [10, 13–15] as well as heavy pairs like D^0 ($c\bar{u}$) and \bar{D}^0 ($\bar{c}u$) [16] has been predicted. The pre-

dicted splitting for the latter is stronger, suggesting a large effect of the magnetic field on heavy quarks due to their early production time and large relaxation time in the medium [16].

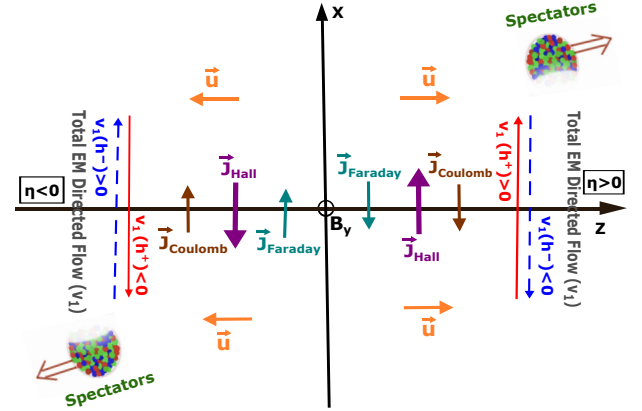


FIG. 1: Diagram (motivated by Refs. [10, 11]) illustrating the influence of the electromagnetic field \vec{B} on v_1 of charged particles from heavy-ion collisions. We use coordinates where the colliding nuclei in $+z$ ($-z$) are located at $+x$ ($-x$), and the generated \vec{B} is along $-y$.

Charge-dependent v_1 splitting between h^+ and h^- in Cu+Au and Au+Au collisions at $\sqrt{s_{NN}} = 200$ GeV [17] was reported by the STAR Collaboration. A large v_1 splitting was observed in Cu+Au, attributed to the stronger Coulomb force in mass-asymmetric Cu+Au compared to Au+Au. A v_1 splitting between h^+ and h^- in Pb+Pb at $\sqrt{s_{NN}} = 5.02$ TeV has been observed by the ALICE Collaboration [18]. Moreover, a large v_1 for D^0 , \bar{D}^0 mesons and a nonzero v_1 splitting between D^0 and \bar{D}^0 has been reported by STAR [19] in Au+Au $\sqrt{s_{NN}} = 200$ GeV and by ALICE [18] in Pb+Pb $\sqrt{s_{NN}} = 5.02$ TeV. During STAR Beam Energy Scan data collection, the Heavy Flavor Tracker detector was absent, and the small heavy flavor production rate at lower than top beam en-

ergy makes it unfeasible to carry out splitting measurements for D^0/\bar{D}^0 .

On the other hand, strange hadrons are measured precisely with the STAR detector setup. Production of s and \bar{s} quarks is enhanced when nuclei collide with sufficient energy to produce quark-gluon plasma [20], yielding relatively abundant strange particles like K , Λ , $\bar{\Lambda}$, ϕ , Ξ and Ω [20, 21]. Due to their low scattering cross sections, thermal freezeout occurs much earlier for the multistrange baryons Ξ and Ω than for particles containing one or no strange quarks [22]; being emitted almost directly from the phase boundary of the hadronizing fireball, they carry important information about the early stages of the collisions [23]. Models [7, 8] predict that v_1 is mostly imparted during this early stage.

The hadrons containing u and d quarks can be either transported from the initial nuclei [24] or produced in the collisions. The transported u and d quarks undergo more interactions, and have different v_1 [25] from the produced u and d quarks or other produced quarks (\bar{u} , \bar{d} , s and \bar{s}). This dependence on origin among u and d quarks complicates the interpretation of splitting arising from EM fields. A significant splitting of proton v_1 slope was recently reported by STAR [26], namely, a change of sign from positive in central collisions to negative in peripheral collisions. If v_1 splitting from transported quarks is independent of centrality, then the negative slope can be interpreted in terms of stronger Faraday+Coulomb over Hall effects in peripheral events.

This analysis exploits hadrons containing only produced quarks [27]. Observation of nonzero v_1 splitting in the absence of transported matter can probe the relative importance of the Hall and Faraday+Coulomb effects [10, 11] with a less complicated interpretation. We measure deviations from the quark coalescence mechanism, whereby collective flow is assumed to be imparted before hadronization, and the observed particles are assumed to form via coalescence of constituent quarks of near-equal momenta. In this scenario, in the limit of small azimuthal anisotropy v_n , the v_n of the resulting hadrons equal the summed v_n for their constituent quarks: $v_1(\text{hadron}) = \sum_i v_1(q_i)$. This is known as the coalescence sum rule, and the number-of-constituent-quark scaling follows from it [24]. Any experimental test of the coalescence sum rule is problematic when u and d quarks are involved, because of the difficulty in distinguishing between transported and produced quarks. Seven qualifying particle species have adequate experimental statistics: $K^-(\bar{u}s)$, $\bar{p}(\bar{u}\bar{u}\bar{d})$, $\bar{\Lambda}(\bar{u}\bar{d}\bar{s})$, $\phi(s\bar{s})$, $\Xi^+(d\bar{s}\bar{s})$, $\Omega^-(sss)$ and $\bar{\Omega}^+(\bar{s}\bar{s}\bar{s})$. Since v_1 is likely sensitive to the constituent quark mass, we combine various particle species into a pair of groups having zero or close-to-zero total mass difference (Δm) at the constituent quark level. We then study the splitting of v_1 as a function of pair charge difference (Δq), which should be sensitive to EM effects, as well as strangeness difference (ΔS). Of course, ΔS is not independent of Δq . With these seven particle species,

there are five independent combinations as shown in Table I, where index-1 shows the identical quark combination case ($\Delta q = \Delta S = 0$) and indices 2-5 are nonidentical quark combinations ($\Delta q \neq 0$ and $\Delta S \neq 0$).

This Letter reports the first measurements of $v_1(y)$ for Ξ and Ω in $\sqrt{s_{\text{NN}}} = 27$ and 200 GeV Au+Au by STAR at RHIC. The main text reports results for 10-40% centrality, where v_1 is the strongest, while 40-80% centrality is covered in the supplemental material. We investigate v_1 splitting between various quark and antiquark combinations versus Δq and ΔS .

The Event Plane Detectors (EPDs), with pseudorapidity acceptance $2.1 < |\eta| < 5.1$ [28] and the Zero-Degree Calorimeter Shower-Maximum Detectors (ZDC-SMDs) with $|\eta| > 6.3$ [29] determine the event plane at $\sqrt{s_{\text{NN}}} = 27$ and 200 GeV, respectively. The STAR Time Projection Chamber (TPC) [30] is used for charged particle tracking within $|\eta| < 1$ and $p_{\text{T}} > 0.2$ GeV/ c . For centrality determination, the probability distributions of uncorrected TPC tracks within $|\eta| < 0.5$ are used. The centrality classes are based on fits to MC Glauber simulations [31–33]. The longitudinal position (V_z) and the radial position (V_r) of the primary vertex are reconstructed from TPC tracks. We require $V_r < 2$ cm, while $|V_z| < 70$ cm at 27 GeV and $|V_z| < 30$ cm at 200 GeV. Tracks must satisfy $p_{\text{T}} > 0.2$ GeV/ c and a distance of closest approach from the primary vertex under 3 cm. We also require tracks to have at least 15 space points in the TPC acceptance ($|\eta| < 1$) and the number of measured space points must be greater than 0.52 times the maximum possible number. Particle identification is based on energy loss in the TPC and time from the Time Of Flight detector [34, 35]. Reliable identification requires $0.4 < p_{\text{T}} < 5$ GeV/ c for p and \bar{p} , and total momentum $p < 1.6$ GeV/ c for π^\pm and K^\pm .

The Λ , $\bar{\Lambda}$, Ξ^- , Ξ^+ , Ω^- and $\bar{\Omega}^+$ candidates within $0.2 < p_{\text{T}} < 5$ GeV/ c are identified by the Kalman filter (KF) method, initially developed for the CBM and ALICE experiments [36–38]. The KF exploits the track fit quality and decay topology. We reconstruct Λ ($\bar{\Lambda}$), Ξ^- (Ξ^+) and Ω^- ($\bar{\Omega}^+$) via $p\pi^-$ ($\bar{p}\pi^+$), $\Lambda\pi^-$ ($\bar{\Lambda}\pi^+$) and ΛK^- ($\bar{\Lambda}K^+$) decay channels, respectively, with $>90\%$ purity. The statistical significance of short-lived particle reconstruction by the KF is improved by $\sim 30\%$ for Ξ^- (Ξ^+) compared to the standard cut-based method [39–41]. The KF also ensures that hyperon candidates do not share daughters with other particles of interest. The ϕ mesons within $0.2 < p_{\text{T}} < 10$ GeV/ c are reconstructed via the invariant mass technique with background subtraction by pair rotation [42].

The v_1 is determined using the event plane method: $v_1 = \langle \cos(\phi - \Psi_1) \rangle / \text{Res}\{\Psi_1\}$, where ϕ is the track azimuthal angle, Ψ_1 is the first-order event plane and $\text{Res}\{\Psi_1\}$ is its resolution [2, 43, 44]. For 10-40% centrality, $\text{Res}\{\Psi_1\}$ is 0.494 and 0.366 at $\sqrt{s_{\text{NN}}} = 27$ and 200 GeV, respectively. We evaluate v_1 differences Δv_1 for all combination pairs listed in Table I, keeping the same ($p_{\text{T}}/n_q, y$) region (where $n_q = 2$ for mesons and

Index	Quark mass	Δq	ΔS	Δv_1 combination	$F_\Delta \times 10^4$ (27 GeV)	$F_\Delta \times 10^4$ (200 GeV)
1	$\Delta m = 0$	0	0	$[\bar{p}(\bar{u}\bar{u}\bar{d}) + \phi(s\bar{s})] - [K^-(\bar{u}s) + \bar{\Lambda}(\bar{u}\bar{d}\bar{s})]$	$03 \pm 43 \pm 13$	$56 \pm 49 \pm 41$
2	$\Delta m \approx 0$	1	2	$[\bar{\Lambda}(\bar{u}\bar{d}\bar{s})] - [\frac{1}{3}\Omega^-(sss) + \frac{2}{3}\bar{p}(\bar{u}\bar{u}\bar{d})]$	$41 \pm 25 \pm 16$	$19 \pm 13 \pm 01$
3	$\Delta m \approx 0$	$\frac{4}{3}$	2	$[\bar{\Lambda}(\bar{u}\bar{d}\bar{s})] - [K^-(\bar{u}s) + \frac{1}{3}\bar{p}(\bar{u}\bar{u}\bar{d})]$	$39 \pm 07 \pm 03$	$16 \pm 05 \pm 03$
4	$\Delta m = 0$	2	6	$[\bar{\Omega}^+(\bar{s}\bar{s}\bar{s})] - [\Omega^-(sss)]$	$83 \pm 130 \pm 25$	$35 \pm 58 \pm 54$
5	$\Delta m \approx 0$	$\frac{7}{3}$	4	$[\bar{\Xi}^+(\bar{d}\bar{s}\bar{s})] - [K^-(\bar{u}s) + \frac{1}{3}\Omega^-(sss)]$	$64 \pm 36 \pm 19$	$26 \pm 20 \pm 04$

TABLE I: Linearly-independent combinations of hadrons whose constituent quarks are all produced. For all combinations, Δm for constituent quarks is zero or near zero, while the charge and strangeness differences vary as tabulated. The measured $F_\Delta = d\Delta v_1/dy$ is also shown. The listed errors are statistical and systematic uncertainties, respectively.

3 for baryons), namely $0.13 < (p_T/n_q) < 1$ GeV/ c and $|y| < 0.8$. For each combination pair, the strength of splitting is characterized by the slope $F_\Delta = d\Delta v_1/dy$.

Systematic uncertainties are estimated by varying the z -vertex cut, track quality cuts and PID cuts. We use Barlow's method [45] to remove statistical fluctuations from the systematic uncertainty. Typical systematic uncertainty in $v_1(y)$, $\Delta v_1(y)$ and $d\Delta v_1/dy$ due to the event, track, and topological cut variations combined is under 5%. We also take into account the systematic uncertainties arising from trigger bias and beam luminosity changes, estimated to be less than 2%. Corrections for TPC tracking efficiency and acceptance are small, and are included in the systematic uncertainty. Systematic uncertainties from all sources are added in quadrature. Systematic uncertainties on the slopes are obtained by fitting for all possible systematic variations and using Barlow's method to get final systematic uncertainties. Nonflow effects (azimuthal correlations unrelated to the reaction plane orientation but arising from resonances, jets, quantum statistics, and final-state interactions) are minimized by the sizable pseudorapidity gap between the TPC and the EPD or ZDC-SMD [1–3, 46–49].

Figure 2 reports the first measurements of Ξ and Ω baryon v_1 for 10-40% centrality in Au+Au at $\sqrt{s_{NN}} = 27$ and 200 GeV. A linear fit $v_1(y) = Fy$ yields slope parameters $10^4 \times F = -214 \pm 79(\text{stat.}) \pm 34(\text{syst.})$ [$-75 \pm 120(\text{stat.}) \pm 17(\text{syst.})$] for Ω^- [$\bar{\Omega}^+$] and $10^4 \times F = -83 \pm 20(\text{stat.}) \pm 0(\text{syst.})$ [$-150 \pm 28(\text{stat.}) \pm 13(\text{syst.})$] for Ξ^- [$\bar{\Xi}^+$] at $\sqrt{s_{NN}} = 27$ GeV.

We first test the coalescence sum rule with identical quark combinations, *i.e.*, the equality $v_1[\bar{p}(\bar{u}\bar{u}\bar{d})] + v_1[\phi(s\bar{s})] = v_1[K^-(\bar{u}s)] + v_1[\bar{\Lambda}(\bar{u}\bar{d}\bar{s})]$ in a common kinematic region $(p_T/n_q, y)$. On both sides, the constituent quark content is $\bar{u}\bar{u}\bar{d}\bar{s}\bar{s}$, so $\Delta m = 0$, $\Delta q = 0$ and $\Delta S = 0$. Then we measure Δv_1 for nonidentical quark combinations $\Delta m \approx 0$, $\Delta q \neq 0$, and $\Delta S \neq 0$. Figure 3 shows the measured $\Delta v_1(y)$ for $(\Delta q, \Delta S) = (0, 0)$ and $(4/3, 2)$ in 10-40% centrality in Au+Au at $\sqrt{s_{NN}} = 27$ GeV. We fit a slope F_Δ assuming $\Delta v_1(y) = F_\Delta y$. For $(\Delta q, \Delta S) = (0, 0)$ (identical quark combinations), the value of the extracted slope is consistent with zero at 10-40% centrality and is about 2 standard deviations from zero at 40-80%

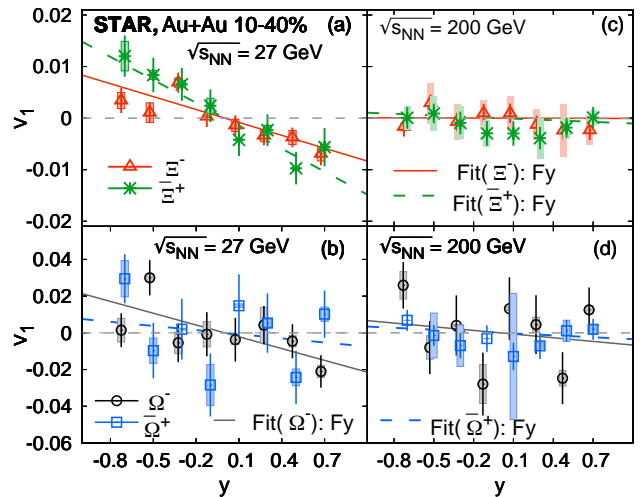


FIG. 2: Directed flow (v_1) of Ξ^- , $\bar{\Xi}^+$, Ω^- and $\bar{\Omega}^+$ versus rapidity (y) for 10-40% Au+Au collisions at $\sqrt{s_{NN}} = 27$ (a, b) and 200 GeV ((c), (d)). The vertical bars and shaded bands denote statistical and systematic uncertainties, respectively. Data points for Ω^- and Ξ^- are staggered horizontally for better visualization.

centrality. This suggests that the coalescence sum rule holds for this identical quark combination (index-1 of Table I) at least for 10-40% centrality. Figure 3 also shows the corresponding dependence on p_T/n_q . For $\Delta q = 0$ and $\Delta S = 0$, Δv_1 versus p_T/n_q is close to zero within measured uncertainties. Therefore, the aforementioned sum rule appears also valid when tested versus p_T/n_q for $\Delta q = \Delta S = 0$.

The fitted F_Δ slopes for all $(\Delta q, \Delta S)$ combinations at 10-40% centrality are listed in Table I. For $(\Delta q, \Delta S) = (4/3, 2)$, the measurement has the best precision, and the increments of Δv_1 with $|y|$ and p_T/n_q are highly significant. This is evident from the lower panels of Fig. 3. As per the discussion of Fig. 1, the increased Δv_1 for $\Delta q \neq 0$ and $\Delta S \neq 0$ may possibly be attributed to the EM field. For 40-80% centrality, the statistical precision does not allow a distinction between $(\Delta q, \Delta S) = (4/3, 2)$ and $(0, 0)$.

In Fig. 4, we display F_Δ at midrapidity for the stud-

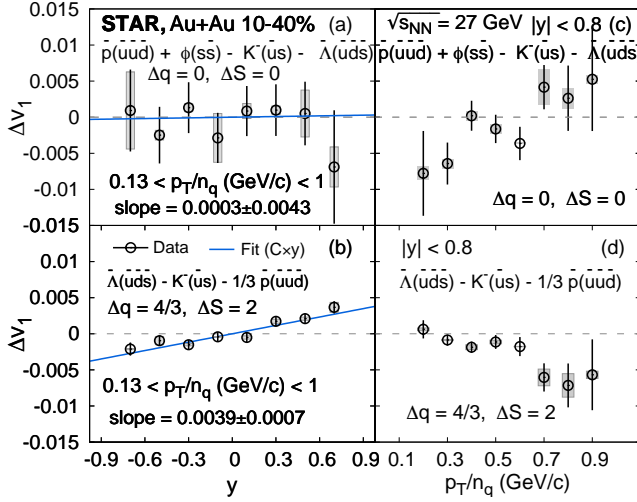


FIG. 3: The Δv_1 as a function of rapidity (a, b) and p_T/n_q (c, d) for $(\Delta q, \Delta S) = (0, 0)$ and $(4/3, 2)$ in 10-40% Au+Au at $\sqrt{s_{NN}} = 27$ GeV. The vertical bars and shaded bands denote statistical and systematic uncertainties, respectively.

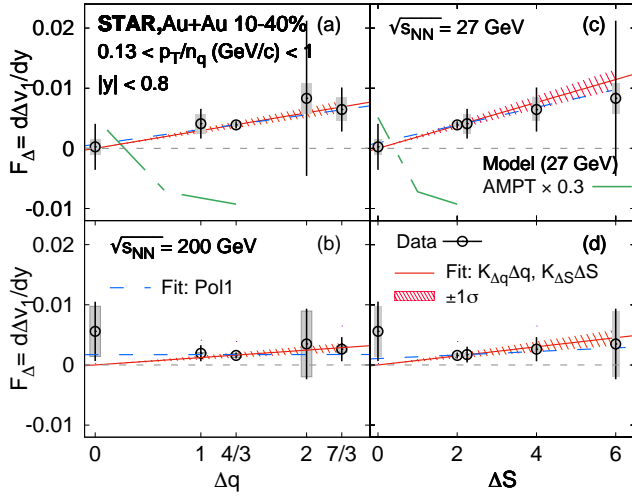


FIG. 4: Midrapidity Δv_1 slope versus Δq (a, b), ΔS (c, d) in 10-40% Au+Au at 27 (a, c) and 200 (b, d) GeV, respectively. The dashed curves show AMPT calculations. The vertical bars and shaded bands denote statistical and systematic uncertainties, respectively. There are two degenerate points at $\Delta S = 2$; one is displaced horizontally for better visualization.

ied combinations as a function of Δq and ΔS in 10-40% central Au+Au at $\sqrt{s_{NN}} = 27$ and 200 GeV. We fit the measurements with a first-order polynomial (shown as blue dashed lines in Fig. 4), and obtain $10^4 \times F_\Delta = (6 \pm 28) + (24 \pm 21)\Delta q$, and $10^4 \times F_\Delta = (17 \pm 21) + (0 \pm 15)\Delta q$ for 10-40% at $\sqrt{s_{NN}} = 27$ and 200 GeV, respectively. For 40-80% centrality, $10^4 \times F_\Delta = (130 \pm 65) + (-77 \pm 49)\Delta q$, and $10^4 \times F_\Delta = (-16 \pm 34) + (27 \pm 25)\Delta q$ at $\sqrt{s_{NN}} = 27$ and 200 GeV, respectively. The intercepts and slope parameters are mostly consistent with zero, given the large uncertainties at 40-80% centrality. Similar conclusions

are reached from the ΔS dependence of $d\Delta v_1/dy$.

Parameters	$\sqrt{s_{NN}} = 27$ GeV	$\sqrt{s_{NN}} = 200$ GeV	Centrality
$K_{\Delta q} (\times 10^4)$	$29 \pm 4.2 \pm 3.7$	$12 \pm 3.3 \pm 2.6$	10-40%
$K_{\Delta S} (\times 10^4)$	$19 \pm 2.8 \pm 2.5$	$7.5 \pm 2.1 \pm 1.4$	10-40%
$K_{\Delta q} (\times 10^4)$	$19 \pm 15 \pm 9.8$	$15 \pm 5.5 \pm 3.0$	40-80%
$K_{\Delta S} (\times 10^4)$	$13 \pm 7.5 \pm 6.5$	$9.5 \pm 3.6 \pm 1.9$	40-80%

TABLE II: Fit parameters for $F_\Delta = K_{\Delta q}\Delta q$, and $F_\Delta = K_{\Delta S}\Delta S$ at 10-40% and 40-80% centrality.

On the other hand, Fig. 4 indicates an overall positive F_Δ . Fitting a constant to the data yields $10^4 \times F_\Delta = 39 \pm 6$ and 17 ± 5 for 10-40% centrality at 27 and 200 GeV, respectively. If the EM field is the underlying physics responsible for this positive splitting, then F_Δ should be proportional to Δq . We therefore assume the sum rule strictly holds, and proceed with linear fits with zero intercepts: $F_\Delta = K_{\Delta q}\Delta q$, and $F_\Delta = K_{\Delta S}\Delta S$. Fit results are shown in Fig. 4. We also show a $\pm 1\sigma$ band around each fit line. The fitted slopes $K_{\Delta q}$ and $K_{\Delta S}$ are tabulated in Table II. The splitting, quantified by the slope F_Δ , increases with Δq and ΔS . The significance of this increasing splitting is 4.8σ for Δq and 4.6σ for ΔS at 27 GeV for 10-40% centrality. For 40-80% centrality, the measurements have poor significance. The splitting evidently increases between $\sqrt{s_{NN}} = 200$ and 27 GeV. The duration of the intense B field increases between 200 and 27 GeV [50]. This effect is expected to result in increased splitting at 27 GeV, as reported here. Our measurements of positive splitting $d\Delta v_1/dy$ for positive Δq is consistent with the expectation of the Hall effect dominating over Coulomb+Faraday in the EM scenario (see Fig. 1).

In Fig. 4 we plot AMPT [51] model calculations and they fail to describe the measurements at $\sqrt{s_{NN}} = 27$ GeV. The AMPT model does not include an EM field.

In summary, we first report the measurements of $v_1(y)$ of multistrange baryons (Ξ and Ω) in Au+Au collisions at $\sqrt{s_{NN}} = 27$ and 200 GeV. We focus on seven produced particle species: K^- , \bar{p} , $\bar{\Lambda}$, ϕ , Ξ^+ , Ω^- and $\bar{\Omega}^+$, none of whose constituent quarks is transported from the colliding nuclei, and study the difference (splitting), $F_\Delta = d\Delta v_1/dy$, between pairs of particle combinations with similar quark content but varying electric charge difference Δq and strangeness difference ΔS . For $\Delta q = \Delta S = 0$, consistency with the coalescence sum rule is observed at 10-40% centrality. For $\Delta q \neq 0$ and $\Delta S \neq 0$, a nonzero average F_Δ is observed with over 5σ significance, dominated by the $(\Delta q, \Delta S) = (4/3, 2)$ pair. This splitting appears to increase with increasing Δq and ΔS . However, the increase is not statistically significant without assuming the coalescence sum rule. With this assumption, the one-parameter linear fit as a function of Δq and ΔS yields a positive slope, respectively 4.8σ and 4.6σ away from zero for $\sqrt{s_{NN}} = 27$ GeV. This splitting is stronger at 27 GeV than at 200 GeV. The

AMPT model (where no EM fields are implemented) fails to describe the data. These midcentral 10-40% data are therefore consistent with electromagnetic effects, where the positive slope suggests a dominance of Hall effect over Faraday+Coulomb effect. Our peripheral 40-80% data statistics are insufficient to yield firm conclusions. On the other hand, a companion analysis [26] by STAR, which considers hadrons involving both produced and transported quarks, finds that in peripheral collisions, Faraday+Coulomb effects dominate the v_1 splitting of hadrons with light (anti-)quarks, such as pions and protons. Additionally, the v_1 splitting of kaons is predominantly influenced by the Hall effect acting on the strange (anti-)quarks. Therefore, the combined inference from Ref. [26] and the present study is that a competition between the Hall effect and the Faraday+Coulomb effect exists, and that the observed pattern of v_1 splitting may be influenced by the particle species and centrality dependence of this competition.

Acknowledgment

We thank the RHIC Operations Group and RCF at BNL, the NERSC Center at LBNL, and the Open Science Grid consortium for providing resources and support. This work was supported in part by the Office of Nuclear Physics within the U.S. DOE Office of Science, the U.S. National Science Foundation, National Natural Science Foundation of China, Chinese Academy of Science, the Ministry of Science and Technology of China and the Chinese Ministry of Education, the Higher Education Sprout Project by Ministry of Education at NCKU, the National Research Foundation of Korea, Czech Science Foundation and Ministry of Education, Youth and Sports of the Czech Republic, Hungarian National Research, Development and Innovation Office, New National Excellency Programme of the Hungarian Ministry of Human Capacities, Department of Atomic Energy and Department of Science and Technology of the Government of India, the National Science Centre of Poland, the Ministry of Science, Education and Sports of the Republic of Croatia, German Bundesministerium für Bildung, Wissenschaft, Forschung und Technologie (BMBF), Helmholtz Association, Ministry of Education, Culture, Sports, Science, and Technology (MEXT) and Japan Society for the Promotion of Science (JSPS).

Appendix A: Supplemental material

1. Results for 40-80% centrality

In Fig. 5, we present the measured $\Delta v_1(y)$ and the corresponding linear fits for $\Delta q = 0$ and $\Delta S = 0$ and for

$\Delta q = 4/3$ and $\Delta S = 2$ in 40-80% centrality in Au+Au collisions at $\sqrt{s_{NN}} = 27$ GeV.

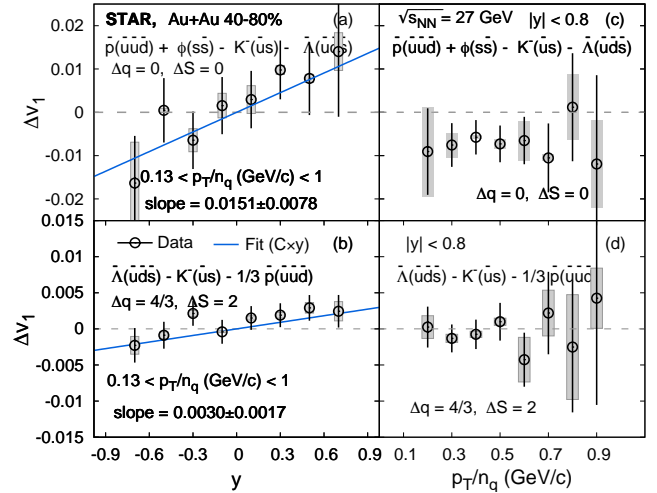


FIG. 5: The Δv_1 as a function of rapidity (a, b) and p_T/n_q (c, d) for $(\Delta q, \Delta S) = (0, 0)$ and $(4/3, 2)$ in 40-80% Au+Au at $\sqrt{s_{NN}} = 27$ GeV. The vertical bars and shaded bands denote statistical and systematic uncertainties, respectively.

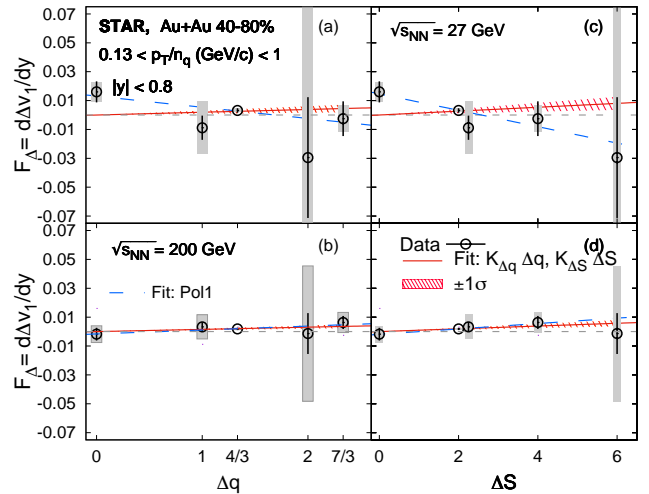


FIG. 6: Midrapidity Δv_1 slope versus Δq (a, b), ΔS (c, d) in 40-80% Au+Au at 27 (a, c) and 200 (b, d) GeV, respectively. The dashed curves show AMPT calculations. The vertical bars and shaded bands denote statistical and systematic uncertainties, respectively. There are two degenerate points at $\Delta S = 2$; one is displaced horizontally for better visualization.

Figure 6 displays F_Δ at midrapidity for the studied combinations as a function of Δq and ΔS in 40-80% central Au+Au collisions at $\sqrt{s_{NN}} = 27$ and 200 GeV. The measurements are dominated by the uncertainties arising from the low abundance of massive hadrons used in the analysis.

-
- [1] S. Voloshin and Y. Zhang, *Z. Phys. C* **70**, 665 (1996).
- [2] A. M. Poskanzer and S. A. Voloshin, *Phys. Rev. C* **58**, 1671 (1998).
- [3] A. Bilandzic, R. Snellings, and S. Voloshin, *Phys. Rev. C* **83**, 044913 (2011).
- [4] P. F. Kolb and U. W. Heinz (2003).
- [5] P. Huovinen and P. V. Ruuskanen, *Ann. Rev. Nucl. Part. Sci.* **56**, 163 (2006).
- [6] H. Sorge, *Phys. Rev. Lett.* **78**, 2309 (1997).
- [7] U. W. Heinz, *Landolt-Bornstein* **23**, 240 (2010).
- [8] S. A. Bass *et al.*, *Prog. Part. Nucl. Phys.* **41**, 255 (1998).
- [9] V. Skokov, A. Y. Illarionov, and V. Toneev, *Int. J. Mod. Phys. A* **24**, 5925 (2009).
- [10] U. Gursoy, D. Kharzeev, E. Marcus, K. Rajagopal, and C. Shen, *Phys. Rev. C* **98**, 055201 (2018).
- [11] U. Gursoy, D. Kharzeev, and K. Rajagopal, *Phys. Rev. C* **89**, 054905 (2014).
- [12] A. Dubla, U. Gürsoy, and R. Snellings, *Mod. Phys. Lett. A* **35**, 2050324 (2020).
- [13] V. Voronyuk, V. D. Toneev, S. A. Voloshin, and W. Cassing, *Phys. Rev. C* **90**, 064903 (2014).
- [14] V. D. Toneev, V. Voronyuk, E. E. Kolomeitsev, and W. Cassing, *Phys. Rev. C* **95**, 034911 (2017).
- [15] L. Oliva, P. Moreau, V. Voronyuk, and E. Bratkovskaya, *Phys. Rev. C* **101**, 014917 (2020).
- [16] S. K. Das, S. Plumari, S. Chatterjee, J. Alam, F. Scardina, and V. Greco, *Phys. Lett. B* **768**, 260 (2017).
- [17] L. Adamczyk *et al.* (STAR), *Phys. Rev. Lett.* **118**, 012301 (2017).
- [18] S. Acharya *et al.* (ALICE), *Phys. Rev. Lett.* **125**, 022301 (2020).
- [19] J. Adam *et al.* (STAR), *Phys. Rev. Lett.* **123**, 162301 (2019).
- [20] J. Rafelski and B. Muller, *Phys. Rev. Lett.* **48**, 1066 (1982), [Erratum: *Phys. Rev. Lett.* **56**, 2334 (1986)].
- [21] A. Shor, *Phys. Rev. Lett.* **54**, 1122 (1985).
- [22] H. van Hecke, H. Sorge, and N. Xu, *Phys. Rev. Lett.* **81**, 5764 (1998).
- [23] J. Adams *et al.* (STAR), *Phys. Rev. Lett.* **92**, 182301 (2004).
- [24] J. C. Dunlop, M. A. Lisa, and P. Sorensen, *Phys. Rev. C* **84**, 044914 (2011).
- [25] Y. Guo, F. Liu, and A. Tang, *Phys. Rev. C* **86**, 044901 (2012).
- [26] **xx**, **xx** (2022), nucl-ex/XXX.
- [27] A. I. Sheikh, D. Keane, and P. Tribedy, *Phys. Rev. C* **105**, 014912 (2022).
- [28] J. Adams *et al.*, *Nucl. Instrum. Meth. A* **968**, 163970 (2020).
- [29] L. Adamczyk *et al.* (STAR), *Phys. Rev. Lett.* **108**, 202301 (2012).
- [30] M. Anderson *et al.*, *Nucl. Instrum. Meth. A* **499**, 659 (2003).
- [31] B. I. Abelev *et al.* (STAR), *Phys. Rev. C* **79**, 034909 (2009).
- [32] M. L. Miller, K. Reygers, S. J. Sanders, and P. Steinberg, *Ann. Rev. Nucl. Part. Sci.* **57**, 205 (2007).
- [33] M. Abdallah *et al.* (STAR), *Phys. Rev. C* **105**, 014901 (2022).
- [34] B. Bonner, H. Chen, G. Eppley, F. Geurts, J. Lamas Valverde, C. Li, W. J. Llope, T. Nussbaum, E. Platner, and J. Roberts, *Nucl. Instrum. Meth. A* **508**, 181 (2003).
- [35] W. J. Llope (STAR), *Nucl. Instrum. Meth. A* **661**, S110 (2012).
- [36] S. Gorbunov, in *On-line reconstruction algorithms for the CBM and ALICE experiments*, *Ph.D. thesis, Johann Wolfgang Goethe-Universität* (2013).
- [37] M. Zyzak, in *Online selection of short-lived particles on manycore computer architectures in the CBM experiment at FAIR*, *Ph.D. thesis, Johann Wolfgang Goethe-Universität* (2016).
- [38] I. Kisel (CBM), *J. Phys. Conf. Ser.* **1070**, 012015 (2018).
- [39] J. Adam *et al.* (STAR), *Phys. Rev. Lett.* **126**, 162301 (2021).
- [40] J. Adam *et al.* (STAR), *Phys. Rev. C* **98**, 014910 (2018).
- [41] J. Adam *et al.* (STAR), *Phys. Rev. C* **102**, 034909 (2020).
- [42] J. Adam *et al.* (ALICE), *Phys. Rev. C* **94**, 054908 (2016).
- [43] J. Adams *et al.* (STAR), *Phys. Rev. C* **73**, 034903 (2006).
- [44] L. Adamczyk *et al.* (STAR), *Phys. Rev. Lett.* **108**, 202301 (2012).
- [45] R. Barlow, in *Conference on Advanced Statistical Techniques in Particle Physics* (2002).
- [46] J.-Y. Ollitrault, *Phys. Rev. D* **46**, 229 (1992).
- [47] G. Agakishiev *et al.* (STAR), *Phys. Rev. C* **85**, 014901 (2012).
- [48] L. Adamczyk *et al.* (STAR), *Phys. Rev. Lett.* **112**, 162301 (2014).
- [49] L. Adamczyk *et al.* (STAR), *Phys. Rev. Lett.* **120**, 062301 (2018).
- [50] L. McLerran and V. Skokov, *Nucl. Phys. A* **929**, 184 (2014).
- [51] K. Nayak, S. Shi, N. Xu, and Z.-W. Lin, *Phys. Rev. C* **100**, 054903 (2019).